2768 *Biochemistry* **2010,** *49,* 2768–2777
DOI: 10.1021/bi100158s

BIOCHEMISTRY
including biophysical chemistry & molecular biology
Accelerated Publication

Mycobacterium tuberculosis Rv0899 Adopts a Mixed α/β-Structure and Does Not Form a Transmembrane β-Barrel[†,‡]

Peter Teriete,[§] Yong Yao,[§] Adrian Kolodzik,[§,⊥] Jinghua Yu,[§] Houhui Song,[∥,@] Michael Niederweis,[∥] and Francesca M. Marassi*[,§]

[§]*Sanford Burnham Medical Research Institute, 10901 North Torrey Pines Road, La Jolla, California 92037, and* [∥]*Department of Microbiology, University of Alabama, Birmingham, Alabama 35294.* [⊥]*Present address: Center for Bioinformatics, University of Hamburg, 20146 Hamburg, Germany.* [@]*Present address: Qingdao Institute of Bioenergy and Bioprocess Technology, Chinese Academy of Sciences, Qingdao, Shandong 266101, P. R. China.*

Received February 2, 2010; Revised Manuscript Received March 2, 2010

ABSTRACT: The membrane protein Rv0899 (OmpATb) from *Mycobacterium tuberculosis*, has been proposed to act as an outer membrane porin and to contribute to the bacterium's adaptation to the acidic environment of the phagosome during infection. The gene is restricted to pathogenic mycobacteria and, thus, is an attractive candidate for the development of anti-tuberculosis chemotherapy. The 326-residue protein contains three domains: an N-terminal domain (residues 1−72) that includes a sequence of 20 hydrophobic amino acids required for membrane translocation, a central B domain (residues 73−200) with homology to the conserved putative lipid-binding BON (bacterial OsmY and nodulation) superfamily, and a C domain (residues 201−326) with homology to the OmpA-C-like superfamily of periplasmic peptidoglycan-binding sequences, found in several types of bacterial membrane proteins, including in the C-terminus of the *Escherichia coli* outer membrane protein OmpA. We have characterized the structure and dynamics of the B and C domains and have determined the three-dimensional structure of the B domain. Rv0899 does not form a transmembrane β-barrel. Residues 73−326 form a mixed α/β-globular structure, encompassing two independently folded modules corresponding to the B and C domains connected by a flexible linker. The B domain folds with three parallel/antiparallel α-helices packed against six parallel/antiparallel β-strands that form a flat β-sheet. The core is hydrophobic, while the exterior is polar and predominantly acidic. The structure of a BON homology domain is revealed here for the first time. In light of this unexpected structure, it is hard to reconcile an outer membrane porin activity with the central domain of the protein. The structure of the B domain and the overall architecture of the protein suggest alternative modes of membrane association.

Tuberculosis (TB) is the seventh most common cause of death globally (*1*). *Mycobacterium tuberculosis*, its causative agent, has achieved a spread in the human population unmatched by any other bacterial pathogen (*2*), despite the availability of effective short-course chemotherapy and the Bacille Calmette-Guerin vaccine. Important factors contributing to the high pathogenicity of *M. tuberculosis* are its highly impermeable cell wall, which prevents the uptake of most hydrophilic antibiotic drugs, and its high adaptability to environmental changes during the course of infection, including nutrient deprivation, hypoxia, various exogenous stress conditions, and the phagosomal environment (*3*).

The complete genome sequence of *M. tuberculosis* H37Rv, the best-characterized strain of the bacterium, has allowed identification of several stress response genes that contribute to pathogenicity (*4*). Among these, the membrane protein Rv0899, encoded by the *rv0899* gene, is thought to confer adaptation of *M. tuberculosis* to the acidic environment of the phagosome (*5*). Sequence analysis of the mycobacterial genomes shows that the gene is restricted to pathogenic mycobacteria associated with TB (*M. tuberculosis* and *Mycobacterium bovis*) and other TB-related diseases (*Mycobacterium marinum*, *Mycobacterium ulcerans*, and *Mycobacterium kansaii*) and, thus, is an attractive candidate for the development of anti-TB chemotherapeutic agents. Notably, two *M. tuberculosis* H37Rv genes (Rv0900 and Rv0901) adjacent to Rv0899 also encode putative membrane proteins and are found exclusively in association with Rv0899 in the same pathogenic mycobacteria, suggesting that the three may constitute an operon dedicated to a common function.

Amino acid sequence analysis reveals that the 326-residue Rv0899 contains three domains (Figure 1). The N-terminal domain (M, residues 1−72) includes a sequence of 20 hydrophobic amino acids (residues 28−50) that is required for membrane translocation but is not cleaved (*6*), thus constituting a

[†]This research was supported by grants from the National Institutes of Health (AI063432 to M.N.; AI074805 to F.M.M. and M.N.; GM075917 to F.M.M.). It utilized NMR Facilities, supported by grants from the National Institutes of Health, at the Sanford Burnham Medical Research Institute (CA030199) and at the University of California at San Diego (S10RR23773). A.K. was supported by a grant from the German Academic Exchange Service.

[‡]The structure coordinates have been deposited in the Protein Data Bank as entry 2KSM.

*To whom correspondence should be addressed: Sanford Burnham Medical Research Institute, 10901 N. Torrey Pines Rd., La Jolla, CA 92037. E-mail: fmarassi@sanfordburnham.org. Phone: (858) 795-5282. Fax: (858) 713-6281.

 Published on Web 03/03/2010

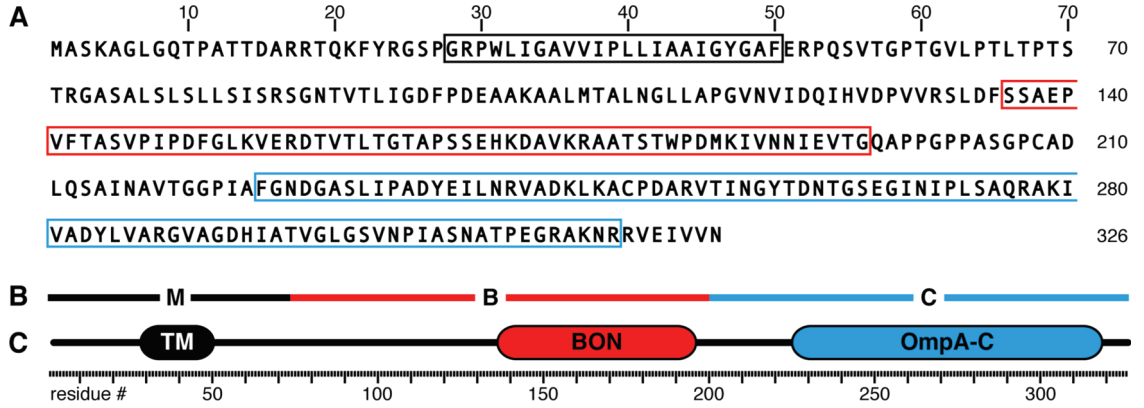

FIGURE 1: Amino acid sequence (A), domain organization (B), and conserved domain homology (C) of *M. tuberculosis* Rv0899. The M domain contains 20 hydrophobic amino acids (residues 28−50) with transmembrane (TM) sequence similarity. The B domain contains a sequence with homology to the BON superfamily (pfam04972, cl02771, residues 136−196). The C domain contains a sequence with homology to the OmpA-C superfamily (pfam00691, cl02931, residues 225−319). The TM, BON, and OmpA-C homology regions are enclosed in black, red, and blue boxes in the sequence, respectively.

membrane anchor. The central domain (B, residues 73−200) shares homology with the BON[1] (bacterial OsmY and nodulation) superfamily (pfam04972), a conserved, putative lipid binding sequence that is found in some osmotic shock protection proteins, secretins, hemolysins, nodulation specificity proteins, and channels (*7*). Finally, the C-terminal domain (C, residues 201−326) has homology to the OmpA-C-like superfamily (pfam00691), a periplasmic peptidoglycan-binding domain that is found in several types of bacterial membrane proteins, including in the C-terminus of outer membrane protein OmpA from *Escherichia coli*. Because of its homology with *E. coli* OmpA, the *rv0899* gene was originally denoted as *ompA* in the published genome sequence of *M. tuberculosis* (*4*), and an outer membrane porin activity was proposed for its protein product, which was subsequently named OmpATb (*8*).

Indeed, Rv0899 was isolated with the mycobacterial cell wall fraction (*6*, *9*), and a pore-forming activity was measured in liposomes and in planar lipid bilayers for purified, recombinant Rv0899 produced in *E. coli* (*6*, *8*, *10*). The N-terminal hydrophobic sequence was found to be required for ion channel activity (*6*, *8*), and proteolytic studies indicated that a trypsin-resistant polypeptide, spanning residues 73−326, was responsible for the pore-forming properties of Rv0899. Furthermore, a polypeptide spanning residues 73−220 was found to be sufficient for inducing the channel characteristics of the native protein in lipid bilayers, when it was expressed as a fusion with the *E. coli* OmpA signal sequence to direct it to its presumed outer membrane location (*10*). Transport experiments further led to the hypothesis that Rv0899 could function as a porin (*5*).

The *rv0899* gene was also shown to be significantly upregulated in wild-type *M. tuberculosis* bacteria exposed to acidic conditions, whereas a mutant, lacking *rv0899*, exhibited a substantially impaired ability to grow at acidic pH in macrophages and in mice (*5*), suggesting that *rv0899* could facilitate the growth of *M. tuberculosis* in a mammalian host by helping it overcome host defense mechanisms. Indeed, pH adaptation is a common trait of pathogenic bacteria (*11*), and it has been shown that mycobacteria, including *M. tuberculosis*, maintain a neutral internal pH in an acidic environment (*12*−*16*). However, the mechanisms utilized by *M. tuberculosis* to adapt to acidic environments are poorly understood. The proposed porin activity and the pH adaption activity of Rv0899 seem to be at odds with each other, since a general response by Gram-negative bacteria to acid stress is to reduce the level of porin expression (*17*−*19*).

To gain further insight into the function of Rv0899, we have characterized the structure and dynamics of residues 73−326, spanning the B and C domains, and have determined the three-dimensional structure of the central B domain, including the BON homology sequence. Rv0899 does not form a transmembrane β-barrel. Residues 73−326 form a globular structure, which encompasses two independently folded modules, corresponding to the B and C domains connected by a flexible linker. Both domains adopt mixed α/β-secondary structures. The B domain adopts a fold that had not been previously documented in the Protein Data Bank (PDB), with three parallel/antiparallel α-helices on one face of the protein, packed against six parallel/antiparallel β-strands that form a β-sheet on the opposite face. The structure reveals the fold of a BON homology domain for the first time. The C domain adopts the typical α/β-structure of peptidoglycan-binding domains in the OmpA-C-like superfamily. The overall architecture of the protein and the unexpected structure of the B domain make it difficult to reconcile a porin activity with its central domain but suggest alternative modes of membrane association. Throughout this work, we refer to the protein as Rv0899, rather than OmpATb, because its homology to *E. coli* OmpA is limited to the C domain and because our studies show that it is not a β-barrel.

MATERIALS AND METHODS

Protein Expression and Purification. Three DNA sequences, each encoding Rv0899 domains B and C (residues 73−326), domain B (residues 73−220), or domain C (residues 196−326), and followed by six C-terminal histidines, were inserted between the NcoI and SwaI sites of the pET-28b expression plasmid (Invitrogen). The resulting plasmids were transformed in *E. coli* BL21(DE3) cells for protein expression. To prepare ^{15}N-labeled and ^{15}N- and ^{13}C-labeled proteins, cells were grown in minimal M9 medium containing $(^{15}NH_4)_2SO_4$ and [^{13}C]glucose (Cambridge Isotope Laboratories). Induction with 1 mM isopropyl 1-thio-β-D-galactopyranoside at 37 °C gave

[1]Abbreviations: BON, bacterial OsmY and nodulation; HSQC, heteronuclear single-quantum correlation; 6-O-PC, 1,2-*O*-dihexyl-*sn*-glycero-3-phosphocholine; 14-O-PC, 1,2-*O*-ditetradecyl-*sn*-glycero-3-phosphocholine; DHPC, 1,2-dihexyl-*sn*-glycero-3-phosphocholine; DPC, dodecylphosphocholine; LPPG, 16:0-lysophosphatidylglycerol; OG, *n*-octyl β-D-glucopyranoside; SDS, sodium dodecyl sulfate.

high-level expression of the polypeptides in the soluble fraction. Cells were lysed using a French press, and the proteins were purified by Ni affinity chromatography (5 mL GE HisTrap FF column), followed by ion exchange chromatography (5 mL GE HiTrap Q FF column). For each polypeptide, protein homogeneity was characterized by MALDI-TOF mass spectrometry, SDS−PAGE, size exclusion chromatography, analytical ultracentrifugation, and NMR spectroscopy. The final yields of purified protein ranged between 2 and 5 mg/L of cell culture. For NMR experiments, the protein solutions were concentrated by ultrafiltration to 0.2−1.0 mM in NMR buffer (5−25 mM $NaH_2(PO_4)$, pH7, 1 mM EDTA, 1 mM DTT).

Analytical Size Exclusion Chromatography. Analytical size exclusion chromatography was performed using a Superdex 75 10/300 column (GE Healthcare) on a Waters HPLC chromatography system with a flow rate of 0.4 mL/min. Protein samples were dissolved in 25 mM sodium phosphate buffer at pH 7 or 4, supplemented with 150 mM NaCl, 1 mM EDTA, and 2 mM DTT, at a concentration of 0.5 mg/mL. The column was calibrated with ovalbumin (43 kDa), chymotrypsinogen (25 kDa), and lysozyme (16 kDa) molecular mass standards.

Analytical Ultracentrifugation. Sedimentation equilibrium experiments were performed using a ProteomeLab XL-I (BeckmanCoulter) analytical ultracentrifuge. Samples containing Rv0899-B and Rv0899-BC polypeptides, at concentrations of 1.00, 0.33, and 0.11 mg/mL, were loaded in six-channel equilibrium cells and centrifuged in an analytical eight-place An-50 Ti rotor, at 30000 rpm and 20 °C for 24 h. The samples also contained 5 mM $NaH_2(PO_4)$ (pH 7) and 1 mM DTT. Data were analyzed using HeteroAnalysis (*20*).

Association with Lipid and Detergents. The association of Rv0899-B with lipid vesicles was tested via addition of 14-O-PC (1,2-*O*-ditetradecyl-*sn*-glycero-3-phosphocholine) vesicles to aqueous solutions of Rv0899-B, in either neutral (pH 7) or acidic (pH 4) buffer, at a 100:1 (protein:lipid) molar ratio. The vesicles were prepared by extrusion through a 100 nm filter, using a Mini-Extruder (Avanti Polar Lipids). To test association with detergents, we added the following to Rv0899-B and Rv0899-BC at concentrations above their respective critical micelle concentrations: 6-O-PC (1,2-*O*-dihexyl-*sn*-glycero-3-phosphocholine), DPC (dodecylphosphocholine), LPPG (16:0-lysophosphatidylglycerol), sodium cholate, OG (*n*-octyl β-D-glucopyranoside), and SDS (sodium dodecyl sulfate). All lipids and detergents were from Avanti Polar Lipids or Anatrace. Refolding in detergent micelles was tested by denaturing Rv0899-B and Rv0899-BC in 6 M urea or 6 M guanidinium hydrochloride, followed by addition of detergent and dialysis using methods previously described for outer membrane proteins (*21*, *22*).

NMR Spectroscopy. NMR experiments were performed at 40 °C on a Bruker AVANCE 600 MHz spectrometer equipped with a cryoprobe or a Bruker AVANCE 800 MHz spectrometer equipped with a standard probe. The NMR data were processed and analyzed using NMRPipe (*23*) and Sparky (*24*).

The backbone ^1H, ^{15}N, and ^{13}C chemical shifts were resolved using two-dimensional $^1H-^{15}N$ and $^1H-^{13}C$ HSQC experiments and assigned using three-dimensional $^1H-^{15}N-^{13}C$ HNCO and HNCA, HN(CO)CA, HN(CA)CO, and HNCACB experiments and three-dimensional ^{15}N- and ^{13}C-edited NOESY-HSQC experiments. Assignments of the side chain resonances were determined with three-dimensional ^{15}N TOCSY-HSQC, ^{13}C NOESY-HSQC, and HCCH-COSY/TOCSY experiments. The NMR experiments are described in the review literature (*25*−*30*).

Homonuclear ^1H NOEs were measured from three-dimensional ^{15}N- and ^{13}C-edited NOESY-HSQC spectra, obtained with mixing times of 100 ms. $^1H-^{15}N$ residual dipolar couplings (RDCs) were measured using in-phase/anti-phase $^{15}N-^1H$ HSQC experiments (*31*) with protein samples in magnetically oriented Pf1 phage (15 mg/mL), fd phage (10 mg/mL, 200 mM KCl), or a compressed 4.5% polyacrylamide gel. Hydrogen−deuterium exchange experiments were performed by dissolving lyophilized protein in buffer with 100% D_2O and then acquiring HSQC spectra at 1 h intervals. $^1H-^{15}N$ heteronuclear NOE measurements were taken using difference experiments with and without 3 s saturation of the ^1H resonances between scans (*32*).

Structure Calculations. Structure calculations were performed using XPLOR-NIH, version 2.24 (*33*). Molecular structures were visualized with PyMol (*34*). Electrostatic potentials were calculated in units of kT/e, where k is Boltzmann's constant, T is the absolute temperature, and e is the proton charge, using PDB2PQR (*35*) and APBS (*36*). All calculations were performed on an eight-core Mac Pro with two 2.8 GHz Quad-Core Intel Xeon processors, running OS X 10.5.8.

A total of 500 structures were generated from extended random coil coordinates using a simulated annealing protocol (*37*), with XPLOR-NIH internal coordinates molecular dynamics (*38*). Backbone ϕ and ψ dihedral angle restraints were derived from analysis of HA, N, C, CA, and CB chemical shifts with the database program TALOS+ (*39*) and were imposed by a quadratic harmonic potential with a force constant of 400 kcal mol^{-1} rad^{-2}. For each statistically significant dihedral angle, the error range was taken directly from the TALOS+ output. Distance restraints derived from NOEs were assigned upper error bounds of 35% and were imposed by a flat-well harmonic potential with a force constant of 40 kcal mol^{-1} $Å^{-2}$. For NOEs involving methyl groups, the error bounds were increased by 0.5 Å per methyl group. For cases in which the NOEs were violated in the first rounds of simulated annealing, the error bound was increased to account for the potential effects of spin diffusion. Hydrogen bond distance restraints were determined from the hydrogen−deuterium exchange data combined with the secondary structure derived from TALOS+ and were imposed by restraining the O−HN distances to 2 ± 0.5 Å and the O−N distances to 3 ± 0.5 Å, with a force constant of 40 kcal mol^{-1} $Å^{-2}$. The torsion angle database Rama potential (*40*) was used, with a force constant of 0.2, to select preferred side chain conformations relative to the backbone dihedral angles. RDC restraints were imposed with the XPLOR-NIH SANI potential with a force constant of 0.01−1.0 kcal/Hz^2 (*41*). Order tensor analysis of the RDC data was performed with the XPLOR-NIH script CalcTensor and with REDCAT (*42*).

The 20 structures with the lowest restraint energies were selected and evaluated using PROCHECK (*43*). The 20 best structures had no dihedral angle violations greater than 5°, no bond angle violations greater than 5°, no NOE distance restraint violations greater than 0.5 Å, and no bond distance violations greater than 0.05 Å. Only 1% of the residues had ϕ and ψ dihedral angles in generously allowed and/or disallowed regions of the Ramachandran plot; these residues are located in the termini outside the structured core of the protein or in connecting loops (Figure S1 of the Supporting Information). Statistics for the resulting family of 20 structures are listed in Table 1. Correlations between experimental and back-calculated RDCs

Table 1: NMR Restraints and Structure Statistics[a]

Experimental Restraints	
dihedral angle	208
NOE distance (Å)	1389
intra	726
short-range	305
medium-range	94
long-range	264
H-bond distance (Å)	29
HN RDC orientation (Hz)	279
Pf1	98
fd	85
compressed gel	96
Root Mean Square Deviation (rmsd)	
experimental restraints	
dihedral angle (deg)	0.659
NOE and H-bond distance (Å)	0.022
HN RDC (Hz)	0.824
idealized covalent geometry	
bonds (Å)	0.002
angles (deg)	0.527
impropers (deg)	0.444
Coordinate Precision[b]	
average pairwise rmsd (Å)	
backbone atoms (C, CA, N, O)	0.82 ± 0.15
all heavy atoms	1.52 ± 0.15
average rmsd from mean (Å)	
backbone atoms	0.57 ± 0.09
heavy atoms	1.05 ± 0.10
Ramachandran Plot ϕ/ψ Angle Statistics[c]	
ϕ and ψ in the most favored regions	78.1%
ϕ and ψ in additionally allowed regions	19.5%
ϕ and ψ in generously allowed regions	1.5%
ϕ and ψ in disallowed regions	1.0%

[a]Calculated for the 20 lowest-energy structures of a total 500 calculated structures. [b]Calculated for the structured core of the protein from residue 80 to 195. [c]Calculated with PROCHECK. Residues with ϕ and ψ in generously allowed or disallowed regions are specified in Figure S1 of the Supporting Information.

are shown in Figure S2 of the Supporting Information. The coordinates have been deposited in the PDB (entry 2KSM).

RESULTS AND DISCUSSION

The B and C Domains of M. tuberculosis Rv0899 form Two Independently Structured Modules. As an initial step toward the structural characterization of *M. tuberculosis* Rv0899, we generated three polypeptides spanning the B and C (Rv0899-BC, residues 73−326), B (Rv0899-B, residues 73−220), and C (Rv0899-C, residues 196−326) domains of the protein. All three were produced in highly purified form as soluble proteins and gave high-resolution NMR spectra in aqueous solution. On SDS−PAGE, each polypeptide migrated with an apparent molecular mass close to that calculated from its amino acid sequence (Figure 2A). SDS−PAGE analysis of full-length Rv0899 extracted from *M. tuberculosis* membranes shows that it also migrates near its calculated molecular mass (33.6 kDa), indicating that the native protein is monomeric or adopts a weak SDS-sensitive oligomeric state (Figure 2B).

To characterize the state of the Rv0899 polypeptides in solution, we used analytical size exclusion chromatography (Figure 2C). The elution profiles show that the three polypeptides elute as predicted from their calculated masses, reflecting their monomeric states in solution. Analytical ultracentrifugation experiments further confirmed them as monomers (not shown).

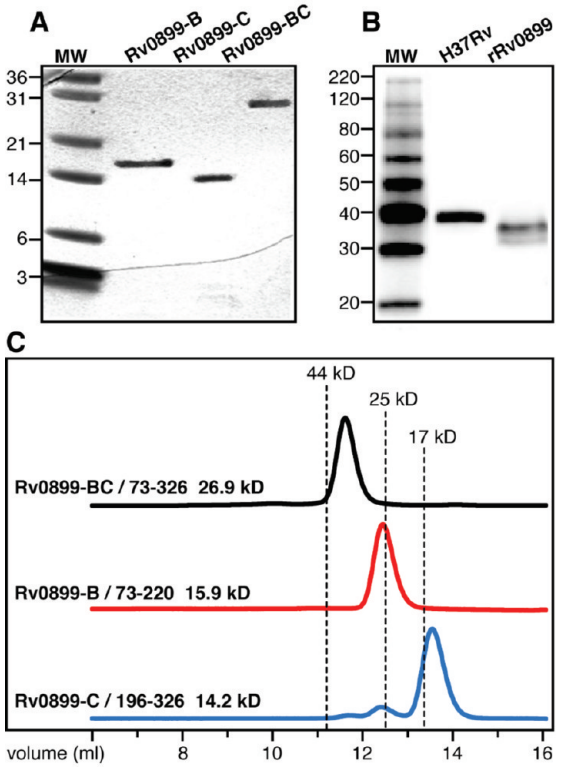

FIGURE 2: Size characterization of Rv0899. (A) SDS−PAGE of recombinant Rv0899 polypeptides used in this study spanning domains B, C, and B and C. (B) Western blot analysis of full-length native Rv0899 expressed in wild-type *M. tuberculosis* (H37Rv) and purified recombinant Rv0899 (rRv0899). Recombinant rRv0899 has a higher electrophoretic mobility than native Rv0899 because it is missing the 44 N-terminal residues in the M domain and has a C-terminal six-histidine tag. Mycobacterial cell extracts obtained with 1% SDS were separated on a 10% SDS−polyacrylamide gel, blotted on a polyvinylidene fluoride membrane, and incubated with Rv0899-specific antiserum (*8*). MagicMarkTM XP Western protein standard was loaded as a control (MW). (C) Size exclusion chromatography showing elution of Rv0899 polypeptides as monomeric species in aqueous solution. The dotted lines indicate elution of specific molecular mass markers.

The solution NMR HSQC spectra of the three constructs are shown in Figure 3. Each spectrum is characterized by uniform resonance line widths and large ^{1}H and ^{15}N chemical shift dispersions, reflecting ordered globular folds for the corresponding polypeptide. Addition of detergents, at concentrations above their respective critical micelle concentrations, had no effect on the spectra and hence no effect on protein conformation (6-O-PC) or resulted in partially collapsed spectra typical of a disordered protein (DPC, LPPG, sodium cholate, octyl glucoside, and SDS). Addition of denaturants (guanidine or urea) resulted in spectra consistent with random coil conformation; however, the native fold could be readily restored after removal of the denaturant by dialysis. Our attempts to refold the polypeptides into detergents, using dialysis reconstitution methods used for β-barrel outer membrane proteins (*21*, *22*), resulted in either the native conformation observed in solution or disordered proteins. Finally, the polypeptides can be lyophilized and rehydrated with no loss of structure. We conclude that the B, C, and BC polypeptides adopt unique conformations in either aqueous or micellar environments.

The three polypeptides are also stable with respect to pH. Rv0899-BC retains its globular fold upon acidification from pH 7 to 4, and the NMR spectrum obtained at pH 4 exhibits only

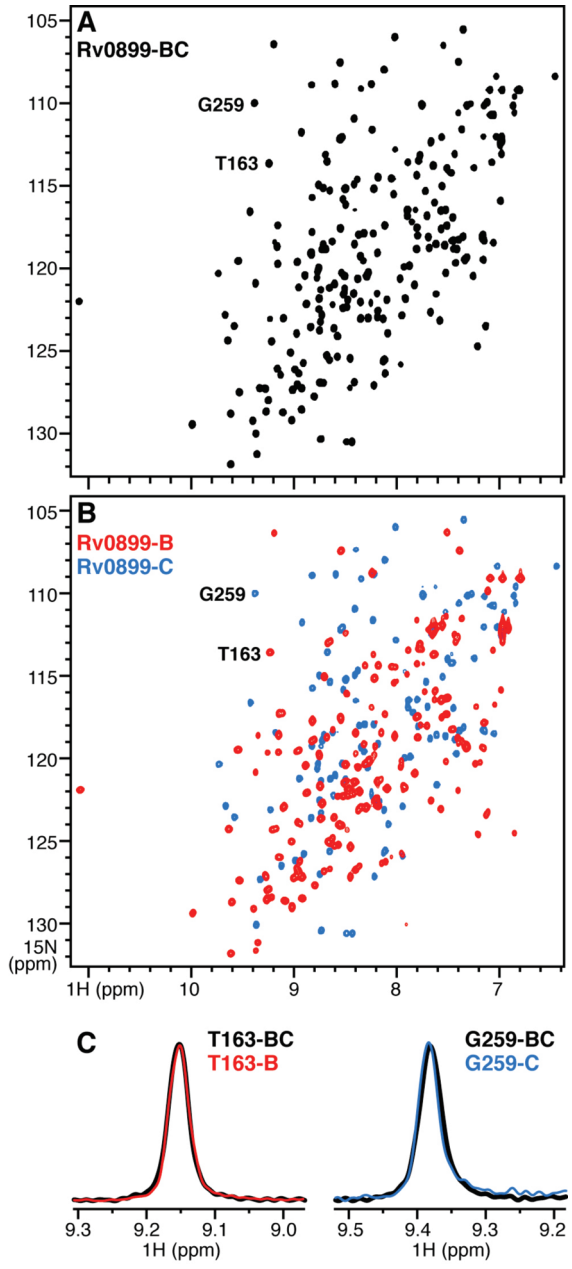

FIGURE 3: Complementary $^{1}H-^{15}N$ HSQC NMR spectra of the soluble B and C domains of Rv0899. (A) Uniformly ^{15}N-labeled Rv0899-BC (residues 73−326). (B) Uniformly ^{15}N-labeled Rv0899-B (red, residues 73−220) and Rv0899-C (blue, residues 196−326). (C) One-dimensional ^{1}H chemical shift slices extracted from the HSQC spectra for peaks corresponding to T163 in the B domain and G259 in the C domain. The four peaks have comparable ^{1}H line widths (16.5 Hz for 163-B, 19.7 Hz for 163-BC, 17.8 Hz for 259-C, and 18.5 Hz for 259-BC).

modest frequency changes consistent with the titration of Asp, Glu, and His residues, and no evidence of unfolding compared to the spectrum at pH 7 (Figures S3 and S4 of the Supporting Information). One residue, Asn111, was found to be susceptible to deamidation over the course of days; however, this did not lead to a conformational change in the protein.

Notably, the spectra of Rv0899-B (Figure 3B, red) and Rv0899-C (Figure 3B, blue) form perfect complementary subsets of the spectrum from Rv0899-BC (Figure 3A), spanning both domains, with the exception of some peaks from residues in the BC connecting region (Figure S5 of the Supporting Information). This demonstrates that the B and C domains constitute independently folded modules, as suggested by sequence homology. The resonance line widths measured in the three spectra are very similar, further indicating that all three polypeptides exist as monomeric species in solution. Since the line widths are not appreciably larger in the spectra of the BC polypeptide, the B and C domains may be significantly dynamically decoupled.

The secondary structure and backbone dynamics of the two independently folded protein domains are shown in Figure 4. The B and C domains adopt mixed α/β-secondary structures that are clearly defined by the chemical shift indices. The αββαβ-structure of the BON homology region is the first to be experimentally determined for a BON sequence and confirms the secondary structure that had been predicted for this superfamily (*7*). The C domain adopts an alternating αβαβαβαβ-structure similar to that of other OmpA-C-like peptidoglycan-binding periplasmic domains (*44*−*46*). Heteronuclear $^{1}H-^{15}N$ NOE measurements are excellent indicators of local backbone motions in proteins and have been used to characterize the dynamics of both globular and membrane proteins. Throughout the structured cores of the B and C domains of the protein, all residues have very similar positive values (near 1) of the $^{1}H-^{15}N$ NOE, reflecting similar backbone dynamics and well-ordered globular structures (Figure 4B). Negative NOEs, reflecting additional backbone motions, are observed for residues connecting the two domains, indicating the presence of a flexible linker between them. Lower NOEs are also observed for residues connecting α1 and β3 in the B domain, which form a more mobile loop.

Three-Dimensional Structure of the B Domain of Rv0899. A high-resolution structure of Rv0899-B was determined by NMR spectroscopy. The structure is composed of six β-strands and three α-helices arranged in the topological order ββαβαββαβ (Figures 5−7). A central four-strand antiparallel β-sheet (β2, β1, β4, and β5) is flanked at each end by a parallel β-strand (β3 and β6), forming a six-strand β-sheet on one face of the structure. The sheet packs against three α-helices, two parallel (α1 and α2) and one antiparallel (α3), on the opposite face. The BON subdomain spans the α2-β4-β5-α3-β6 sequence in the C-terminal half of the structure (Figures 5−7, red).

The connecting loops (L1−L8) are relatively short, except for the longer L4, which has significant β-strand secondary structure. The loops are all as ordered as the core of the protein, with the exception of L3, linking α1 to β3, which is significantly more dynamic as evidenced by its lower value of the heteronuclear NOE (Figure 4B). The Asn111-Gly112 amino acid pair, located at the end of α1 and preceding L3, undergoes in vitro deamidation, a pH-dependent reaction whereby Asn is converted to Asp and ammonia is released. Asparagine residues preceding glycine, and situated in conformationally flexible regions of proteins, are frequently deamidated, with potentially significant consequences for protein regulation and function (*47*). In the case of Rv0899, deamidation and the concomitant release of ammonia could have important consequences for the acid adaptation function of the protein. Whether Asn111 deamidation is functional in vivo remains to be determined. The sequence of Rv0899 contains an additional Asn-Gly pair in the C domain (Asn258-Gly259), as well as a C-terminal Asn; however, no evidence of deamidation was detected for these residues.

The 1:2 ratio of juxtaposed α:β structures (α-helices to β-strands) results in a flat rather than curved β-sheet, and a boxlike structure measuring approximately 30 Å × 30 Å × 15 Å along each side (Figure 6). The core of the Rv0899 B domain is hydrophobic, while the exterior is polar and predominantly

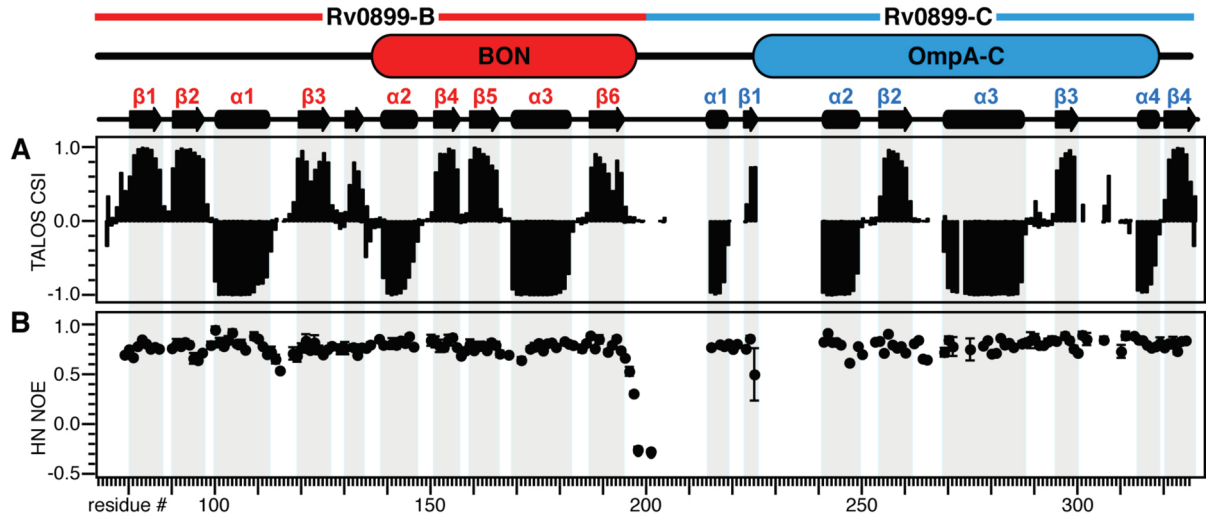

FIGURE 4: Secondary structure and backbone dynamics of the Rv0899 B and C domains. (A) Chemical shift index determined from TALOS+ analysis. (B) $^{1}H-^{15}N$ heteronuclear NOEs. Positions that are left blank correspond to proline residues, overlapped resonances, or unassigned resonances. Domain organization, homology to the BON (red) and OmpA-C (blue) superfamilies, and secondary structures are shown at the top.

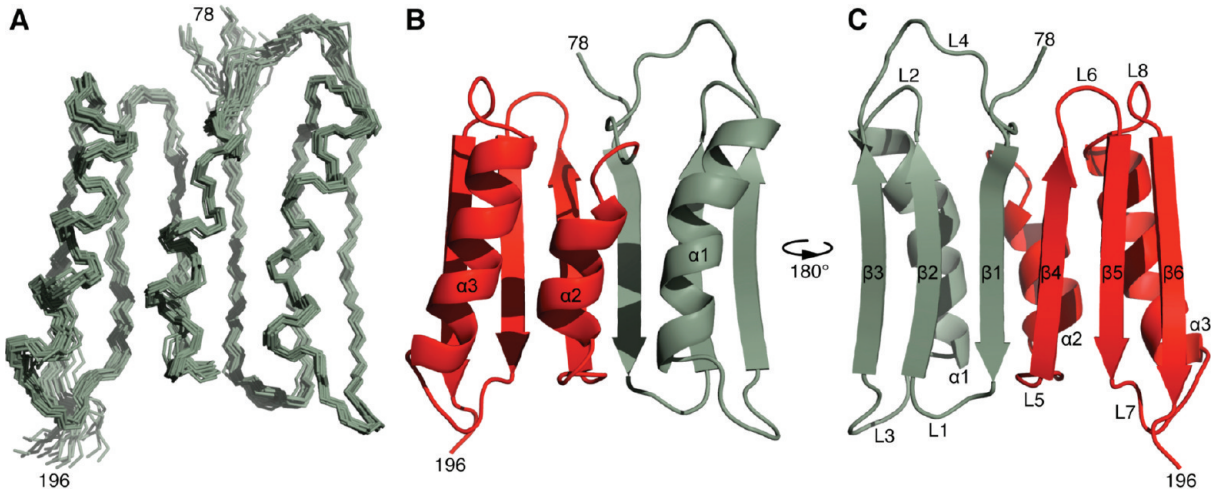

FIGURE 5: Solution structure of the B domain of *M. tuberculosis* Rv0899. The structured core extends from residue 80 to 195. (A) Backbone (C, CA, and N) representation of the 20 lowest-energy structures. In the structured core, the average pairwise rmsd is 0.82 Å for the backbone (C, CA, N, and O) atoms and 1.52 Å for all heavy atoms. (B and C) Ribbon representations showing 180° views of the structure. The three α-helices (α1−α3), six *β*-strands (*β*1−*β*6), and eight loops (L1−L8) are labeled. The BON subdomain (α2-*β*4-*β*5-α3-*β*6) is colored red.

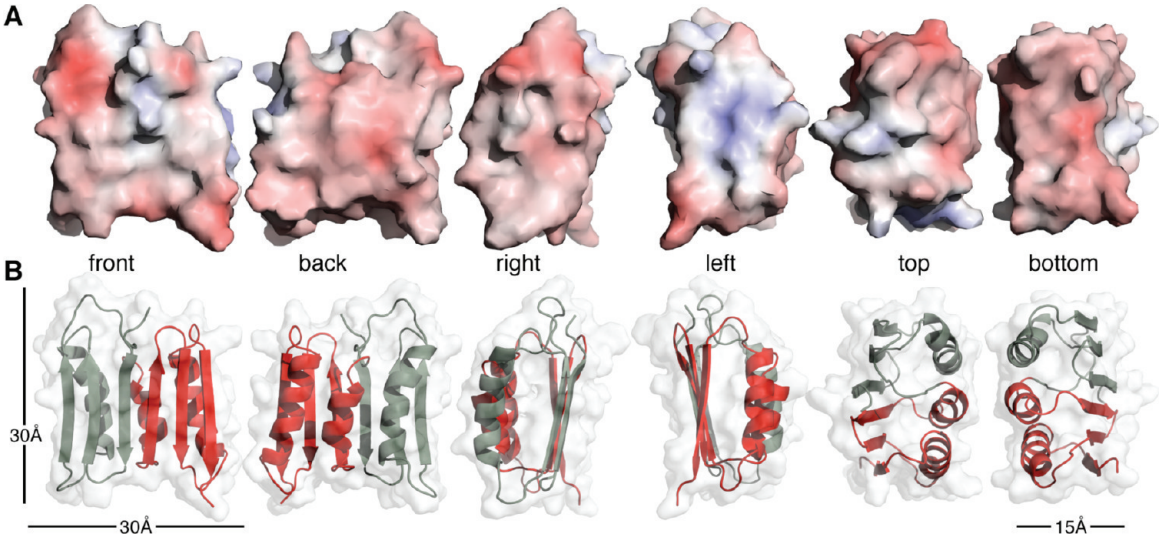

FIGURE 6: Electrostatic surface properties of *M. tuberculosis* Rv0899-B. (A) Electrostatic potential isocontours are shown at $8k_BT$ (blue) and $-8k_BT$ (red), where k_B is Boltzmann's constant and and T is the temperature. (B) The corresponding backbone representations show the BON homology colored red.

acidic, except for two areas of positive charge caused by Lys154 protruding from the upper middle region of the β-sheet (Figure 6, front), and by Lys172, Lys176, Arg177, and Lys187 protruding from the side of the BON homology subdomain (Figure 6, left).

The structure of the B domain is formed by two topologically similar subdomains, a BON subdomain (Figure 7, red) and an N-terminal subdomain with significant BON-like features (Figure 7, gray). The two subdomains are symmetric about α2, and their backbone atoms can be aligned with a root-mean-square deviation (rmsd) of 1.8 Å, by performing a 180° rotation of either one around an axis normal to the six-strand β-sheet (Figure 7B−D). The $\alpha\beta\beta\alpha\beta$-secondary structure of the BON homology subdomain is as predicted in the original description of this superfamily, on the basis of sequence alignment (*7*). Notably, the BON-like subdomain shares both a similar topology (β1-β2-α1-β3), except for the missing first α-helix, and significant amino acid sequence homology with the BON superfamily (Figure 8). In particular, the fully conserved glycine, which is a defining BON feature, is found in both the BON (Gly164) and BON-like (Gly95) subdomains, at similar positions in both their amino acid sequences and structural topologies (Figures 7 and 8) Thus, the structure of Rv0899-B may be viewed as being formed by two BON homology subdomains connected in antiparallel (Figure 7).

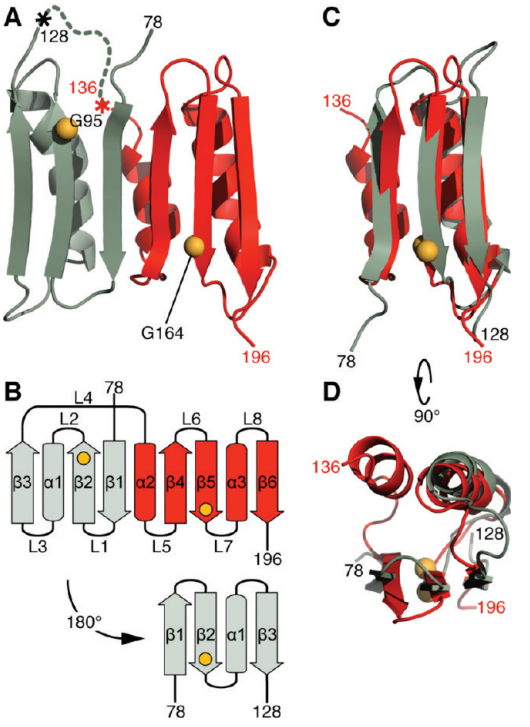

FIGURE 7: Structure and topology of *M. tuberculosis* Rv0899-B showing the BON (red, residues 136−196) and BON-like (gray, residues 78−128) homology subdomains. Conserved glycines (G95 and G164) are shown as yellow spheres (CA atoms). (A) Arrangement of BON and BON-like subdomains in the protein structure. (B) Topology of Rv0899-B. The BON and BON-like topologies are similar except for the initial BON helix (α2). (C and D) Superposition of BON and BON-like subdomains. The pairwise rmsd for backbone heavy atoms is 1.81 Å.

Implications for the Biological Function of Rv0899. The amino acid sequence of the BON superfamily was first identified by bioinformatic gene analysis in bacterial osmotic shock resistance protein OsmY, a family of hemolysins, a group of nodulation specificity proteins, secretory channels, mechano-sensitive channels, the cell wall peptidoglycan-binding LysM domain, and several hypothetical proteins (*7*). It is characterized by a conserved glycine residue and several conserved hydrophobic regions (Figure 8). The lack of catalytic residues in the sequence alignment led the authors to propose that it is a binding domain with mechanical, rather than catalytic, functionality, and annotation in the literature suggests that it interacts with phospholipid membranes (*7*).

OsmY is a hyperosmotically induced periplasmic or outer membrane protein (*48*). The BON domains in OsmY have been proposed to help prevent cell shrinkage by contacting the phospholipid interfaces surrounding the periplasmic space and physically attaching the inner membrane to the more rigid outer membrane. Mechano-sensitive ion channels have also been implicated in osmotic regulation, and some appear to function in response to membrane deformation (*49*). Their BON domains

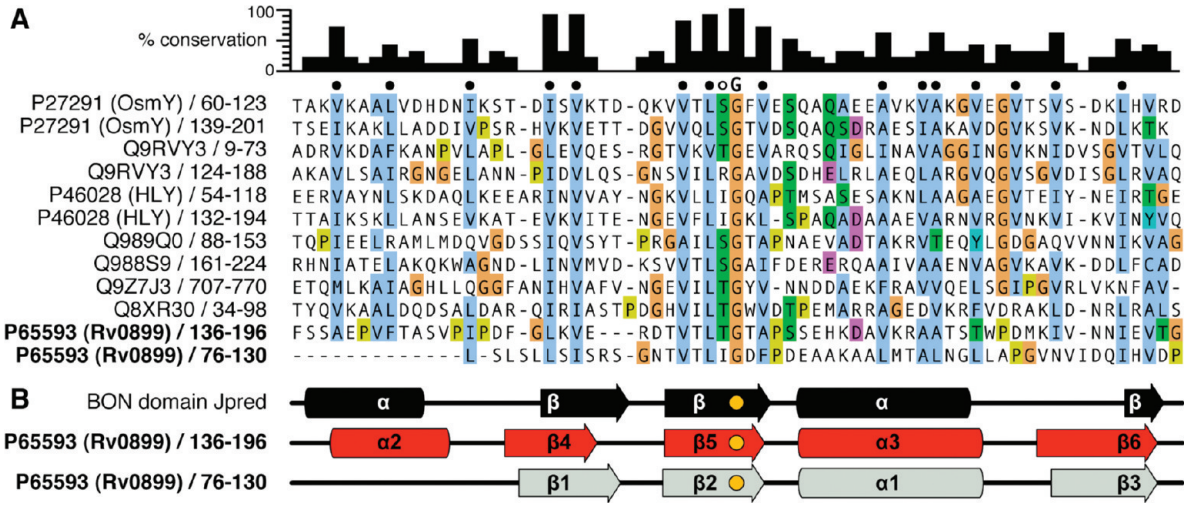

FIGURE 8: Amino acid sequence alignment and secondary structure of representative BON domains (*7*), including Rv0899 BON (residues 136−196) and BON-like (residues 76−130) sequences. UniProt identifiers are given for each sequence. (A) Amino acid conservation, and sequence alignment, produced with ClustalW (*62*) and rendered with Jalview (*63*) using ClustalX coloring (*62*). Fully conserved glycines are marked with a G, conserved hydrophobic residues with filled circles, and conserved Ser/Thr residues with empty circles. (B) Secondary structures predicted for the representative BON domains (black) using Jpred (*64*) or determined in this study for the BON (red) and BON-like (gray) subdomains of Rv0899. Yellow circles denote conserved glycines.

have been proposed to react to deformations in the plasma membrane and signal to the ion channel domain (*7*). In the case of Rv0899, the highly polar surface of the protein suggests that it may not be active in lipid binding at neutral pH but could associate with lipids at acidic pH (pH <4), where surface Asp and Glu residues are expected to be protonated and uncharged. We examined this possibility by adding DMPC vesicles to aqueous solutions of Rv0899-B at either neutral (pH 7) or acidic (pH 4) pH. No evidence of binding was observed in either case; however, this should be examined further with different lipids as binding may require a specific headgroup, chain length, or lipid type.

Analysis of the NCBI database, using BLAST (*50*) and CDART (*51*), indicates that the individual BON and OmpA-C-like homology domains are widespread in a variety of amino acid sequences from diverse organisms. However, there are only few unique sequences with the BON−OmpA-C combination. Notably, they occur in other bacteria (e.g., *Burkholderia*) that like *M. tuberculosis* need to adapt to unusually harsh environments. However, no structures have been characterized for any of these proteins.

A DALI (*52*) search for similar folds in the Protein Data Bank yielded no structures with the complete BON and BON-like arrangement observed for Rv0899-B. However, the BON $\alpha\beta\beta\alpha\beta$-fold is found in several functionally diverse proteins, including metal binding protein domains, metal binding methyltransferases, members of the type III bacterial secretion system, and osmotic shock-induced proteins, with DALI *Z* scores as high as 3.7. The structural similarity to metal binding polypeptides is intriguing. In these cases, the metals are typically coordinated by a combination of His, Asp, Glu, Ser, Thr, and aromatic residues. Rv0899-B possesses only two His residues at opposite ends of the β-sheet, too far apart to act in concert, but several Asp, Glu Ser, Thr, and aromatic residues are situated such that they could participate in a metal binding function.

Implications for the Organization of Rv0899 in the Mycobacterial Membranes. While typical outer membrane proteins exist as transmembrane β-barrels, with an apolar lipid-facing exterior and a hydrophilic interior (*53*), Rv0899 adopts a globular α/β-structure for ~80% of its amino acid sequence (residues 73−326) and is not a β-barrel. The outer membrane localization and porin function of Rv0899 were originally predicted on the basis of homology to the C-terminus of *E. coli* OmpA and later reinforced by fractionation studies and measurements of channel and porin activities (*5*, *6*, *8*, *10*).

The C domain of Rv0899 has distinct homology to the OmpA-C superfamily of bacterial peptidoglycan-binding domains and may be predicted to stabilize the mycobacterial cell envelope by binding the peptidoglycan layer. However, it is important to note that OmpA-C homology domains are all periplasmic and are found in integral outer membrane proteins (e.g., OmpA, which inserts in the outer membrane as a β-barrel), as well as outer membrane lipoproteins (e.g., PAL, which is bound to the outer membrane through a lipid anchor), and integral inner membrane proteins (e.g., MotB, which is inserted in the inner membrane through a transmembrane helix) (*53*). Thus, homology to OmpA-C in itself is not sufficient to classify Rv0899 as an outer membrane protein. Throughout this work, we refer to the protein as Rv0899 precisely for this reason.

Several studies suggested that Rv0899 localizes to the outer membrane of *M. tuberculosis*. Subcellular separation experiments showed that full-length Rv0899 expressed in *M. smegmatis* and *M. bovis* BCG fractionates with the mycobacterial outer membrane (*6*, *54*), although a significant amount was also found in the soluble protein fraction (*6*), while deletion of the hydrophobic sequence in the protein's N-terminal M domain resulted in a water-soluble protein devoid of any channel forming activity in the liposome swelling assay (*6*, *8*). The latter was interpreted to reflect protein mislocalization due to the missing signal sequence. Furthermore, a polyclonal rabbit antiserum raised to the N-terminally truncated protein recognized a protein of similar molecular mass in detergent extracts of broken *M. tuberculosis* cells (*8*), and Rv0899 expressed in *M. bovis* BCG was found to be accessible to proteases and antibodies, indicating cell surface expression (*55*).

Nevertheless, both periplasmic and inner membrane proteins can have significant interactions with the cell wall and often fractionate with it. Indeed, isolated outer membranes often contain subsurface contaminants, and demonstrating that the outer membrane fraction is free of inner membrane and periplasmic components is not straightforward; thus, the observation of a polypeptide in the cell wall fraction is not in itself sufficient evidence of outer membrane localization (*53*, *56*). In the case of Rv0899, the periplasmic peptidoglycan-binding C domain would certainly strengthen the protein's interactions with the outer membrane and potentially cause it to separate with that fraction. The Tromp1/TroA protein, from the syphilis spirochete *Treponema pallidum*, is a notable example of misassignment to the outer membrane. Tromp1 was originally predicted to be a major outer membrane porin, based on its ability to form channels in planar bilayer assays and fractionation studies. Later, it was shown to be a periplasmic protein anchored to the bacterial inner membrane with an α/β-fold that is inconsistent with outer membrane insertion (*53*, *56*, *57*). This could also be the case for Rv0899, and the possibility that Rv0899 is anchored to the inner membrane should not be ignored at this stage.

It is possible that the physiological function of Rv0899 is not related to a porin activity. On the other hand, Rv0899 has been shown to be required for the rapid adaptation of *M. tuberculosis* to acidic environments (*5*). Interestingly, a recent study of *M. tuberculosis* acid stress response genes indicates that the same mechanisms that confer acid resistance also provide protection against other forms of extracellular stress, including mechanical stress, reinforcing the important role of the *M. tuberculosis* cell envelope in protection against diverse stresses (*14*). Such a function would be consistent with either inner or outer membrane localization.

The mycobacterial cell envelope is composed of chemically distinct layers that include a lipid inner membrane (IM), two periplasmic layers (L1 and L2; at least one is composed of peptidoglycan/arabinogalactan polymers), and an asymmetric lipid outer membrane (OM) that contains a mixture of phospholipids and mycolic acids (*58*). The exterior of the envelope is further coated by a polysaccharide capsule (*59*). The 20-residue N-terminal transmembrane domain of Rv0899 is sufficiently long to traverse either the inner or outer mycobacterial lipid membranes. Although most outer membrane proteins form transmembrane β-barrels, there are some that insert as transmembrane α-helices (*60*, *61*). For example, Wza, the translocon for *E. coli* capsular saccharides, forms an octameric α-helical barrel in the outer membrane and extends into the periplasmic space connecting to the peptidoglycan layer through three soluble domains (*60*).

The three-domain architecture of Rv0899, the structure of its B domain, the conformation of its C domain, and the presence of a hydrophobic transmembrane sequence suggest four possible

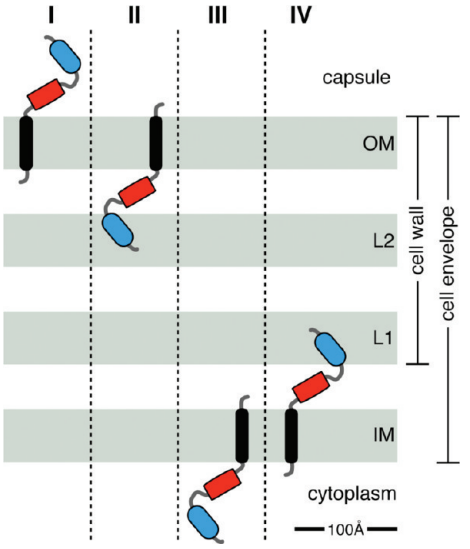

FIGURE 9: Four possible models for the organization of Rv0899 in the mycobacterial cell envelope. Rv0899 is shown as a monomer with its transmembrane M (black), B (red), and C (blue) domains. The four layers forming the mycobacterial cell envelope are colored gray. They correspond to an asymmetric lipid bilayer outer membrane (OM), two periplasmic layers (L1 and L2) composed in part of peptidoglycan/arabinogalactan polymers, and a lipid bilayer inner membrane (IM) facing the cytoplasm. The capsule coating the cell exterior is composed primarily of polysaccharides. The dimensions of the membranes and periplasmic layers are taken from ref *58*. The model of Rv0899 is drawn to scale with the dimensions of the B domain (30 Å × 30 Å × 15 Å) determined from its solution structure.

model arrangements of the protein within the mycobacterial envelope, involving insertion of the N-terminal transmembrane helix across the outer or inner membranes (Figure 9). Models I and II are both consistent with localization of Rv0899 to the mycobacterial outer membrane. However, model I, which exposes the B and C domains of the protein to the cellular exterior, is unlikely, since both the amino acid sequence and secondary structure of the C domain place it in the category of periplasmic peptidoglycan-binding domains. Model II is similar to the Wza architecture and places the B and C domains of the proteins in the periplasm where they would be able to interact with one (L2) or potentially both (L1 and L2) peptidoglycan layers. Models III and IV, in contrast, localize the protein to the inner membrane. Of these, model III is not very likely since it would place the periplasmic peptidoglycan-binding C domain in the cytoplasm, where its function would be questionable. Model IV, on the other hand, is possible and would be similar to the Tromp1/TroA architecture. Distinguishing between the two most likely arrangements (models II and IV) of the protein in the mycobacterial cell envelope will require additional functional and structural studies to understand the exact function and organization of Rv0899.

ACKNOWLEDGMENT

We thank Philip Draper for providing the Rv0899-specific antiserum, Stanley Opella for providing purified Pf1 and fd bacteriophages, and Andrey Bobkov for his assistance with analytical centrifugation.

SUPPORTING INFORMATION AVAILABLE

Dihedral angles in disallowed or generously allowed regions of the Ramachandran plot (Figure S1), correlation between experimental and back-calculated RDCs (Figure S2), effect of a lower pH on the conformation of Rv0899 (Figures S3 and S4), and chemical shift differences between Rv0899-BC and Rv0899-B or Rv0899-C (Figure S5). This material is available free of charge via the Internet at http://pubs.acs.org.

REFERENCES

1. Mathers, C. D., Boerma, T., and Ma Fat, D. (2009) Global and regional causes of death. *Br. Med. Bull. 92*, 7–32.
2. Cook, G. M., Berney, M., Gebhard, S., Heinemann, M., Cox, R. A., Danilchanka, O., and Niederweis, M. (2009) Physiology of mycobacteria. *Adv. Microb. Physiol. 55*, 81–182.
3. Ehrt, S., and Schnappinger, D. (2009) Mycobacterial survival strategies in the phagosome: Defence against host stresses. *Cell. Microbiol. 11*, 1170–1178.
4. Cole, S. T., Brosch, R., Parkhill, J., Garnier, T., Churcher, C., Harris, D., Gordon, S. V., Eiglmeier, K., Gas, S., Barry, C. E., III, Tekaia, F., Badcock, K., Basham, D., Brown, D., Chillingworth, T., Connor, R., Davies, R., Devlin, K., Feltwell, T., Gentles, S., Hamlin, N., Holroyd, S., Hornsby, T., Jagels, K., Krogh, A., McLean, J., Moule, S., Murphy, L., Oliver, K., Osborne, J., Quail, M. A., Rajandream, M. A., Rogers, J., Rutter, S., Seeger, K., Skelton, J., Squares, R., Squares, S., Sulston, J. E., Taylor, K., Whitehead, S., and Barrell, B. G. (1998) Deciphering the biology of *Mycobacterium tuberculosis* from the complete genome sequence. *Nature 393*, 537–544.
5. Raynaud, C., Papavinasasundaram, K. G., Speight, R. A., Springer, B., Sander, P., Bottger, E. C., Colston, M. J., and Draper, P. (2002) The functions of OmpATb, a pore-forming protein of *Mycobacterium tuberculosis*. *Mol. Microbiol. 46*, 191–201.
6. Alahari, A., Saint, N., Campagna, S., Molle, V., Molle, G., and Kremer, L. (2007) The N-terminal domain of OmpATb is required for membrane translocation and pore-forming activity in mycobacteria. *J. Bacteriol. 189*, 6351–6358.
7. Yeats, C., and Bateman, A. (2003) The BON domain: A putative membrane-binding domain. *Trends Biochem. Sci. 28*, 352–355.
8. Senaratne, R. H., Mobasheri, H., Papavinasasundaram, K. G., Jenner, P., Lea, E. J., and Draper, P. (1998) Expression of a gene for a porin-like protein of the OmpA family from *Mycobacterium tuberculosis* H37Rv. *J. Bacteriol. 180*, 3541–3547.
9. Song, H., Sandie, R., Wang, Y., Andrade-Navarro, M. A., and Niederweis, M. (2008) Identification of outer membrane proteins of *Mycobacterium tuberculosis*. *Tuberculosis 88*, 526–544.
10. Molle, V., Saint, N., Campagna, S., Kremer, L., Lea, E., Draper, P., and Molle, G. (2006) pH-dependent pore-forming activity of OmpATb from *Mycobacterium tuberculosis* and characterization of the channel by peptidic dissection. *Mol. Microbiol. 61*, 826–837.
11. Foster, J. W. (1999) When protons attack: Microbial strategies of acid adaptation. *Curr. Opin. Microbiol. 2*, 170–174.
12. Zhang, Y., Scorpio, A., Nikaido, H., and Sun, Z. (1999) Role of acid pH and deficient efflux of pyrazinoic acid in unique susceptibility of *Mycobacterium tuberculosis* to pyrazinamide. *J. Bacteriol. 181*, 2044–2049.
13. Rao, M., Streur, T. L., Aldwell, F. E., and Cook, G. M. (2001) Intracellular pH regulation by *Mycobacterium smegmatis* and *Mycobacterium bovis* BCG. *Microbiology 147*, 1017–1024.
14. Vandal, O. H., Roberts, J. A., Odaira, T., Schnappinger, D., Nathan, C. F., and Ehrt, S. (2009) Acid-susceptible mutants of *Mycobacterium tuberculosis* share hypersusceptibility to cell wall and oxidative stress and to the host environment. *J. Bacteriol. 191*, 625–631.
15. Vandal, O. H., Nathan, C. F., and Ehrt, S. (2009) Acid resistance in *Mycobacterium tuberculosis*. *J. Bacteriol. 191*, 4714–4721.
16. Vandal, O. H., Pierini, L. M., Schnappinger, D., Nathan, C. F., and Ehrt, S. (2008) A membrane protein preserves intrabacterial pH in intraphagosomal *Mycobacterium tuberculosis*. *Nat. Med. 14*, 849–854.
17. Thomas, A. D., and Booth, I. R. (1992) The regulation of expression of the porin gene ompC by acid pH. *J. Gen. Microbiol. 138*, 1829–1835.
18. Samartzidou, H., Mehrazin, M., Xu, Z., Benedik, M. J., and Delcour, A. H. (2003) Cadaverine inhibition of porin plays a role in cell survival at acidic pH. *J. Bacteriol. 185*, 13–19.
19. Begic, S., and Worobec, E. A. (2006) Regulation of *Serratia marcescens* ompF and ompC porin genes in response to osmotic stress, salicylate, temperature and pH. *Microbiology 152*, 485–491.
20. Cole, J. L., and Lary, J. W. (2005) HeteroAnalysis, University of Connecticut, Storrs, CT.
21. Vogt, J., and Schulz, G. E. (1999) The structure of the outer membrane protein OmpX from *Escherichia coli* reveals possible mechanisms of virulence. *Structure 7*, 1301–1309.

22. Arora, A., Abildgaard, F., Bushweller, J. H., and Tamm, L. K. (2001) Structure of outer membrane protein A transmembrane domain by NMR spectroscopy. *Nat. Struct. Biol. 8*, 334–338.
23. Delaglio, F., Grzesiek, S., Vuister, G. W., Zhu, G., Pfeifer, J., and Bax, A. (1995) NMRPipe: A multidimensional spectral processing system based on UNIX pipes. *J. Biomol. NMR 6*, 277–293.
24. Goddard, T. D., and Kneller, D. G. (2004) SPARKY 3, University of California, San Francisco.
25. Fesik, S. W., and Zuiderweg, E. R. (1990) Heteronuclear three-dimensional NMR spectroscopy of isotopically labelled biological macromolecules. *Q. Rev. Biophys. 23*, 97–131.
26. Bax, A., and Grzesiek, S. (1993) Methodological advances in protein NMR. *Acc. Chem. Res. 26*, 131–138.
27. Cavanagh, J., Fairbrother, W. J., Palmer, A. G., and Skelton, N. J. (1996) Protein NMR spectroscopy: Principles and practice, Academic Press, San Diego.
28. Clore, G. M., and Gronenborn, A. M. (1998) NMR structure determination of proteins and protein complexes larger than 20 kDa. *Curr. Opin. Chem. Biol. 2*, 564–570.
29. Ferentz, A. E., and Wagner, G. (2000) NMR spectroscopy: A multifaceted approach to macromolecular structure. *Q. Rev. Biophys. 33*, 29–65.
30. Kay, L. E. (2001) Nuclear magnetic resonance methods for high molecular weight proteins: A study involving a complex of maltose binding protein and β-cyclodextrin. *Methods Enzymol. 339*, 174–203.
31. Ottiger, M., Delaglio, F., and Bax, A. (1998) Measurement of J and dipolar couplings from simplified two-dimensional NMR spectra. *J. Magn. Reson. 131*, 373–378.
32. Farrow, N. A., Zhang, O., Forman-Kay, J. D., and Kay, L. E. (1994) A heteronuclear correlation experiment for simultaneous determination of ^{15}N longitudinal decay and chemical exchange rates of systems in slow equilibrium. *J. Biomol. NMR 4*, 727–734.
33. Schwieters, C. D., Kuszewski, J. J., Tjandra, N., and Clore, G. M. (2003) The Xplor-NIH NMR molecular structure determination package. *J. Magn. Reson. 160*, 65–73.
34. DeLano, W. L. (2005) PyMol, DeLano Scientific, San Carlos, CA.
35. Dolinsky, T. J., Nielsen, J. E., McCammon, J. A., and Baker, N. A. (2004) PDB2PQR: An automated pipeline for the setup of Poisson-Boltzmann electrostatics calculations. *Nucleic Acids Res. 32*, W665–W667.
36. Baker, N. A., Sept, D., Joseph, S., Holst, M. J., and McCammon, J. A. (2001) Electrostatics of nanosystems: Application to microtubules and the ribosome. *Proc. Natl. Acad. Sci. U.S.A. 98*, 10037–10041.
37. Nilges, M., Clore, G. M., and Gronenborn, A. M. (1988) Determination of three-dimensional structures of proteins from interproton distance data by dynamical simulated annealing from a random array of atoms. Circumventing problems associated with folding. *FEBS Lett. 239*, 129–136.
38. Schwieters, C. D., and Clore, G. M. (2001) Internal coordinates for molecular dynamics and minimization in structure determination and refinement. *J. Magn. Reson. 152*, 288–302.
39. Shen, Y., Delaglio, F., Cornilescu, G., and Bax, A. (2009) TALOS+: A hybrid method for predicting protein backbone torsion angles from NMR chemical shifts. *J. Biomol. NMR 44*, 213–223.
40. Kuszewski, J., Gronenborn, A. M., and Clore, G. M. (1997) Improvements and extensions in the conformational database potential for the refinement of NMR and X-ray structures of proteins and nucleic acids. *J. Magn. Reson. 125*, 171–177.
41. Clore, G. M., Gronenborn, A. M., and Tjandra, N. (1998) Direct structure refinement against residual dipolar couplings in the presence of rhombicity of unknown magnitude. *J. Magn. Reson. 131*, 159–162.
42. Valafar, H., and Prestegard, J. H. (2004) REDCAT: A residual dipolar coupling analysis tool. *J. Magn. Reson. 167*, 228–241.
43. Laskowski, R. A., MacArthur, M. W., Moss, D. S., and Thornton, J. M. (1993) PROCHECK: A program to check the stereochemical quality of protein structures. *J. Appl. Crystallogr. 26*, 283.
44. Grizot, S., and Buchanan, S. K. (2004) Structure of the OmpA-like domain of RmpM from *Neisseria meningitidis*. *Mol. Microbiol. 51*, 1027–1037.
45. Parsons, L. M., Lin, F., and Orban, J. (2006) Peptidoglycan recognition by Pal, an outer membrane lipoprotein. *Biochemistry 45*, 2122–2128.
46. Roujeinikova, A. (2008) Crystal structure of the cell wall anchor domain of MotB, a stator component of the bacterial flagellar motor: Implications for peptidoglycan recognition. *Proc. Natl. Acad. Sci. U.S.A. 105*, 10348–10353.
47. Weintraub, S. J., and Deverman, B. E. (2007) Chronoregulation by asparagine deamidation. *Sci. STKE 2007*, No. re7.
48. Yim, H. H., and Villarejo, M. (1992) osmY, a new hyperosmotically inducible gene, encodes a periplasmic protein in *Escherichia coli*. *J. Bacteriol. 174*, 3637–3644.
49. Perozo, E., Kloda, A., Cortes, D. M., and Martinac, B. (2002) Physical principles underlying the transduction of bilayer deformation forces during mechanosensitive channel gating. *Nat. Struct. Biol. 9*, 696–703.
50. Altschul, S. F., and Gish, W. (1996) Local alignment statistics. *Methods Enzymol. 266*, 460–480.
51. Geer, L. Y., Domrachev, M., Lipman, D. J., and Bryant, S. H. (2002) CDART: Protein homology by domain architecture. *Genome Res. 12*, 1619–1623.
52. Holm, L., and Sander, C. (1993) Protein structure comparison by alignment of distance matrices. *J. Mol. Biol. 233*, 123–138.
53. Nikaido, H. (2003) Molecular basis of bacterial outer membrane permeability revisited. *Microbiol. Mol. Biol. Rev. 67*, 593–656.
54. Rezwan, M., Laneelle, M. A., Sander, P., and Daffe, M. (2007) Breaking down the wall: Fractionation of mycobacteria. *J. Microbiol. Methods 68*, 32–39.
55. Song, H., Sandie, R., Wang, Y., Andrade-Navarro, M. A., and Niederweis, M. (2008) Identification of outer membrane proteins of *Mycobacterium tuberculosis*. *Tuberculosis 88*, 526–544.
56. Akins, D. R., Robinson, E., Shevchenko, D., Elkins, C., Cox, D. L., and Radolf, J. D. (1997) Tromp1, a putative rare outer membrane protein, is anchored by an uncleaved signal sequence to the *Treponema pallidum* cytoplasmic membrane. *J. Bacteriol. 179*, 5076–5086.
57. Lee, Y. H., Deka, R. K., Norgard, M. V., Radolf, J. D., and Hasemann, C. A. (1999) *Treponema pallidum* TroA is a periplasmic zinc-binding protein with a helical backbone. *Nat. Struct. Biol. 6*, 628–633.
58. Hoffmann, C., Leis, A., Niederweis, M., Plitzko, J. M., and Engelhardt, H. (2008) Disclosure of the mycobacterial outer membrane: Cryo-electron tomography and vitreous sections reveal the lipid bilayer structure. *Proc. Natl. Acad. Sci. U.S.A. 105*, 3963–3967.
59. Draper, P., and Daffe, M. (2005) The cell envelope of *Mycobacterium tuberculosis* with special reference to the capsule and outer permeability barrier. In Tuberculosis and the tubercle bacillus (Cole, S. T., Eisenach, K. D., McMurray, D. N., and Jacobs, W. R., Jr., Eds.) pp 261−273, American Society for Microbiology Press, Washington, DC.
60. Dong, C., Beis, K., Nesper, J., Brunkan-Lamontagne, A. L., Clarke, B. R., Whitfield, C., and Naismith, J. H. (2006) Wza the translocon for *E. coli* capsular polysaccharides defines a new class of membrane protein. *Nature 444*, 226–229.
61. Chandran, V., Fronzes, R., Duquerroy, S., Cronin, N., Navaza, J., and Waksman, G. (2009) Structure of the outer membrane complex of a type IV secretion system. *Nature 462*, 1011–1015.
62. Thompson, J. D., Higgins, D. G., and Gibson, T. J. (1994) CLUSTAL W: Improving the sensitivity of progressive multiple sequence alignment through sequence weighting, position-specific gap penalties and weight matrix choice. *Nucleic Acids Res. 22*, 4673–4680.
63. Clamp, M., Cuff, J., Searle, S. M., and Barton, G. J. (2004) The Jalview Java alignment editor. *Bioinformatics 20*, 426–427.
64. Cole, C., Barber, J. D., and Barton, G. J. (2008) The Jpred 3 secondary structure prediction server. *Nucleic Acids Res. 36*, W197–W201.